Macromolecules **2014,** 47, (24), 8833-8845

Graphene/Hyperbranched-Polymer Nanocomposites: Insight from Molecular Dynamics Simulations

Kostas Karatasos

Laboratory of Physical Chemistry, Department of Chemical Engineering,

Aristotle University of Thessaloniki,

54124 Thessaloniki, Greece

Abstract

We explore by means of Molecular Dynamics (MD) simulations mixtures of graphene with hyperbranched polyesters (Boltorn ®) of two different pseudo-generations in a wide range of temperatures. Static and dynamic features of the polymeric component are probed in order to assess the effects of the presence of graphene in the polymer's behavior, while we also examine the structural rearrangement of the graphene sheets in the presence of a non-crystallizable highly-branched polymeric component. Our results show that graphene platelets are forming stacks comprised by a small number of flakes (typically 2 to 3) which are dispersed within the polymeric matrix. The characteristics of the spatial arrangement of the graphene planes and that of the formed clusters (including their relative orientation) depend sensitively on the temperature and on the size of the hyperbranched component. From the dynamic point of view, a significant slowing down is detected both in local and in global polymer dynamics in composite systems. The strong dynamic slowing down is accompanied by the occurrence of a glass-like transition at a considerably higher temperature compared to that characterizing the respective pristine polymer systems.

We believe that the results reported in the present study capture also generic characteristics of the behavior of such materials and therefore could be exploited for a better control of the mechanical and thermal characteristics of hyperbranched polymer/graphene systems in a more general aspect.

Tel.: +30-2310-995850; fax: +30-2310-996222; e-mail: karatas@eng.auth.gr

I. Introduction

Fabrication of polymer-based composite materials with low cost, high processability, and enhanced performance remains among the main challenges in materials science. There is a plethora of different formulations such as polymer/clay mixtures[1], nanoparticles dispersed in a polymer matrix[2] and polymeric systems with carbon-nanotube and graphite-based inclusions[3, 4] among others, in an effort to produce materials with tailor-made properties and optimal cost-to-performance ratio.

Among the soft components, hyperbranched polymers have emerged as promising candidates for such composites owing to their unique properties[5-8]. These molecules are cheap since they can be synthesized in one-pot synthesis protocols[9], they are multifunctional due to the large number of functional groups in a rather small volume and they possess advantageous processing capabilities due to their lower viscosity compared to the same molecular weight linear polymers[10]. In general, these materials are also characterized by a high thermal stability and by the absence of crystallization or entanglement effects that are common in linear polymers and which may affect the composites' performance[11].

In this work we have focused on the detailed study by means of fully atomistic molecular dynamic simulations of nanocomposite materials comprised by a specific category of commercially available dendritic molecules, namely hyperbranched polyesters (Boltorn ®)[12, 13] and graphene, a material known to possess excellent mechanical, thermal, electric and gas barrier properties, with lower cost of production compared to other carbon-based fillers[14, 15]. Use of hyperbranched polyesters such as those studied here in polymer/filler hybrids has recently been described in a variety of different systems demonstrating their capacity to enhance stability, increase functionality and improve the performance of the resulted composite materials[16-22]. On the other hand, numerous efforts are devoted on the exploitation of the properties of graphene towards the fabrication of mechanically reinforced, thermally resilient and highly conductive composites[23-29]. Therefore, it is expected that combination of the advantageous features of these two components may result in high-end materials with superb physical properties while keeping the cost low. Although, to our knowledge, hyperbranched polyester/graphene composites have not as yet been studied experimentally, recent efforts examining the utilization of other

hyperbranched polymers in the control of graphite-oxide dispersion[30] and the production of graphene-based composites[31, 32], demonstrate the potential arising from the combination of the properties of such constituents towards the fabrication of molecularly-designed hybrid materials with improved properties.

The detail afforded by fully atomistic computer simulations can contribute decisively towards a deeper understanding of the elementary mechanisms which operate in microscopic scale and are intimately related to the manifestation of the macroscopic physical properties of nanocomposite materials[33, 34]. In the present study we attempt to describe the details of the graphene spatial arrangement within the hyperbranched polymer matrix, its role in the modification of the thermal behavior of the composites and the implications of its presence in the static and dynamic properties of the polymeric components. In addition, we examine the role of the size/morphology of the polymer molecules and we propose mechanisms which can interpret the observed behavior and can potentially be checked by appropriate experimental techniques, such as differential scanning calorimetry, X-ray diffractometry, neutron scattering and dielectric spectroscopy, among others.

To remain close to realistic conditions, we have chosen to simulate multi-graphene/multi-polymer composites mimicking the situation of materials produced by melt mixing at high temperatures which are then brought at lower temperatures by gradual cooling.

II. Systems' details and simulation protocol

To examine the case of relatively high graphene loading which can lead to an improved reinforcement ability in the composites[35] and in order to explore the effects of a constricted environment not only for the local polymer motions but also for the global dynamics of the branched molecules, we have simulated systems comprised by an equal number of graphene flakes and hyperbranched polyesters. Furthermore, in order to allow for a reasonable degree of interdiffusion between the two components of the mixtures, we have opted in examining graphene sheets with lateral length comparable to the average size of the hyperbranched polymers, i.e., with dimensions of 15Å×15Å (see section IV.1 for details on the determination of the polyesters' average dimensions). Namely, we have constructed two models each comprised by 20 hyperbranched molecules and 20 graphene sheets as summarized in table I. Although the size of the graphene sheets used in the present study is smaller than the μm-sized

flakes commonly met in relevant applications, recent advances in the graphene-production protocols have enabled the fabrication of nm-sized graphene flakes (see ref [36] and references therein), rendering thus polymer-graphene nanocomposites physically realizable. Furthermore, based on the generic nature of most of the physical aspects of the behavior observed in the present models, we believe that analogous composites where both the graphene and the average size of the hyperbranched polymers are scaled-up proportionally in molecular size, would exhibit similar properties.

Table I: details on the composition of the simulated systems

System	Number of HB molecules	Number of graphene sheets	volume fraction of graphene (v/v %)
H20/GRA	20	20	21.8
H30/GRA	20	20	13.5

Scheme 1 depicts the chemical details of the H20 and H30 hyperbranched polyesters.

For the parameterization of the bonded and non-bonded interactions between atoms of the hyperbranched polyesters we have followed that described in our earlier work for the pristine polymers[31] (which was based on the AMBER forcefield[37]), where it was shown that available experimental data were satisfactorily reproduced. Forcefield details for graphene were also adopted from the AMBER set of parameters corresponding to generic aromatic carbon atoms (atomtype CA), in line with recent fully atomistic molecular dynamics simulations studies, examining properties of pristine graphene[38-40] or complexes of graphene with other macromolecular compounds[41-43].

The initial structure of the models were constructed by the aid of the package Packmol[44]. Following the construction of the initial configurations, the systems were subjected to an annealing procedure with successive heating steps of 50K, from 300K to 700K. At each temperature energy minimization with combined steepest descent and conjugate gradient cycles was performed, followed by isobaric-isothermal (NPT) MD simulations (ranging between 20ns and 90ns in trajectory length with a step of 1fs, depending on temperature). Production trajectories in the NPT ensemble were generated in the cooling procedure which followed, starting from 700K down to

300K with 50K steps. Again, at each temperature combined energy minimization and NPT MD equilibration cycles of several tens of ns (depending on temperature) were performed, until several energetic parameters and static/thermodynamic properties of the two components (density of the mixture, radius of gyration of the hyperbranched polyesters and other characteristics of the spatial arrangement of the two components in the mixture) were stabilized.

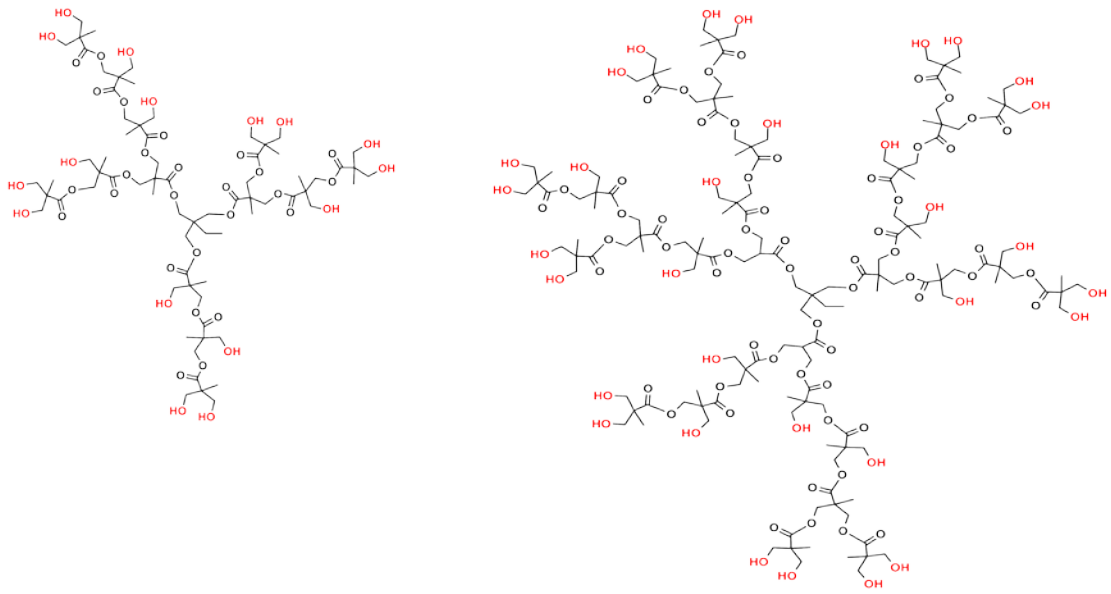

Scheme1: Chemical details of the hyperbranched polyesters. H20 (Mw=1749,8 g/mol), left and H30 (Mw=3607.6 g/mol), right.

Scheme 2 shows a graphical representation of a graphene sheet together with the partial charges assigned to its edge carbons.

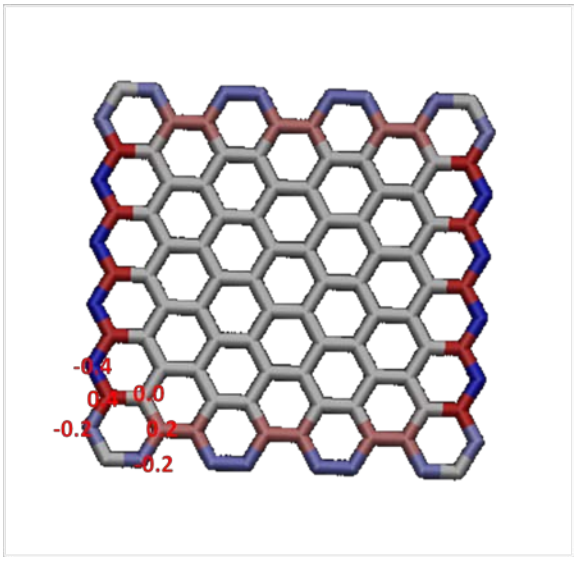

Scheme 2: A graphical impression of the graphene sheet used in the nanocomposites. The carbon atoms are shown in the rod representation. Partial charges in |*e*| assigned to the edge carbons are also shown, following ref [45].

Ensuing the equilibration at each temperature, the NPT production runs were performed with 1fs step and 1ps saving frequency at a pressure of 1 bar. Temperature control was achieved by employing the Langevin method (with a damping coefficient of $3ps^{-1}$), while the Nose-Hoover Langevin piston method[46] was employed for the control of pressure (using a piston period of 0.1 ps and a decay time of 0.05 ps). Electrostatic interactions were computed via the particle mesh Ewald (PME) scheme.[47] All simulations were conducted with NAMD 2.9[48] using periodic boundary conditions and with a distance cutoff at 12Å.

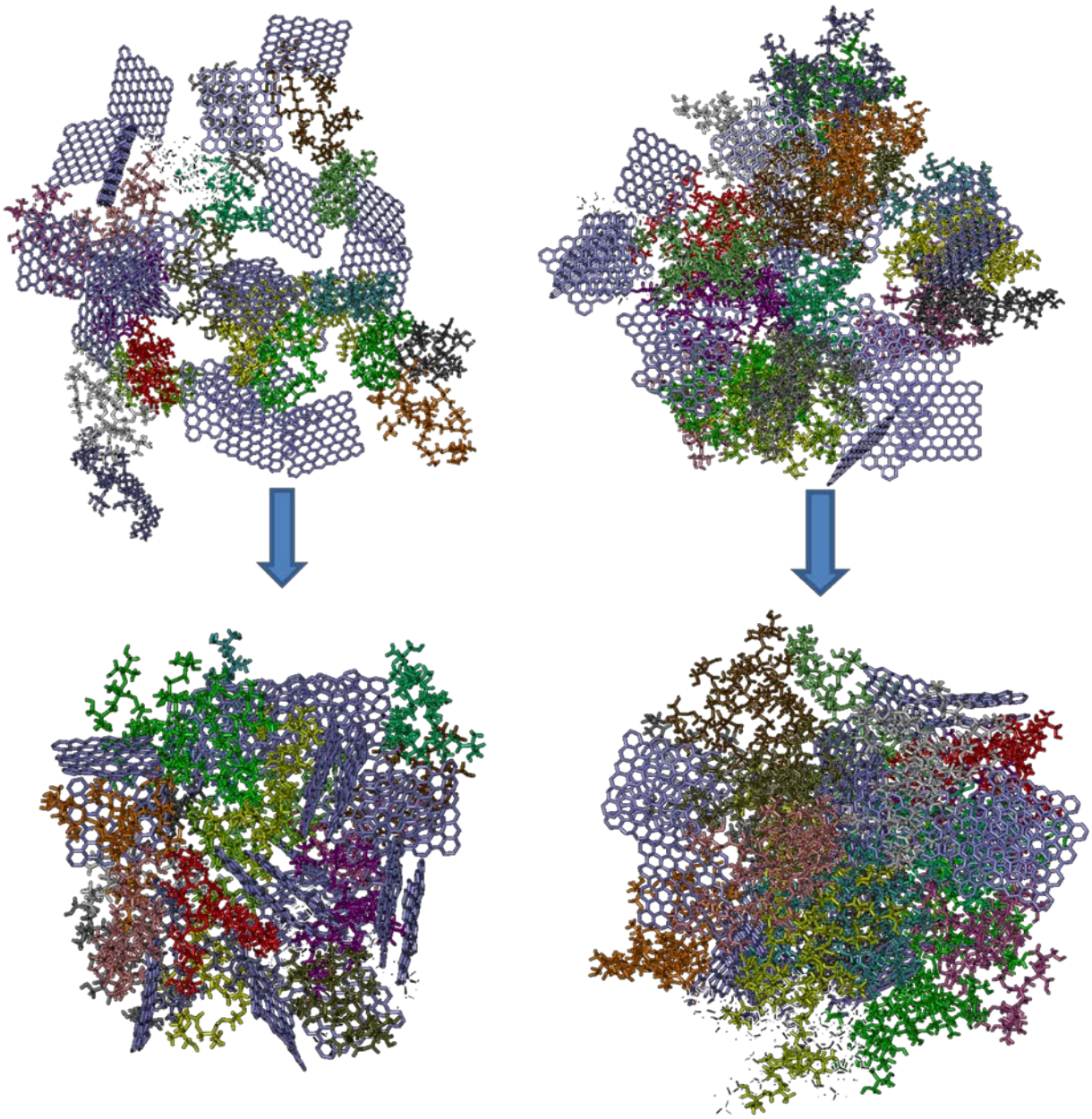

Figure 1: Initial configurations (upper panel) and equilibrated structures prior to the production runs (lower panel) for the examined models (H20/GRA in left and H30/GRA in right) at T=700K. Each molecule of the hyperbranched polyester is shown in different color for better visual impression of the polymer dispersion in the mixture.

Figure 1 depicts initial configurations of the two models (prior to the annealing procedure) and equilibrated states at T=700K prior to the commencement of the production runs at that temperature.

As shown in the snapshots of the systems after equilibration, the graphene platelets appear with a rough rather than a perfectly planar surface, in line with theoretical[49-51] predictions and experimental observations[51, 52]. Therefore, hereafter whenever we refer to a graphene plane, we will assume a definition based on the two principal axes

of inertia of that graphene platelet which define a plane that is essentially parallel to the original planar surface. Similarly, the direction of a graphene platelet will be defined via the third principal axes of inertia which is perpendicular to those defining the graphene plane.

III. Thermal behavior of the systems

The response of the composites to thermal treatment is a key issue pertinent to their industrial use[53] and is closely related to structural details and dynamic processes down to the microscopic scale[54]. To examine characteristic changes imparted to the samples upon temperature variation, we have monitored the dependence of their specific volume as a function of temperature, as shown in figure 2.

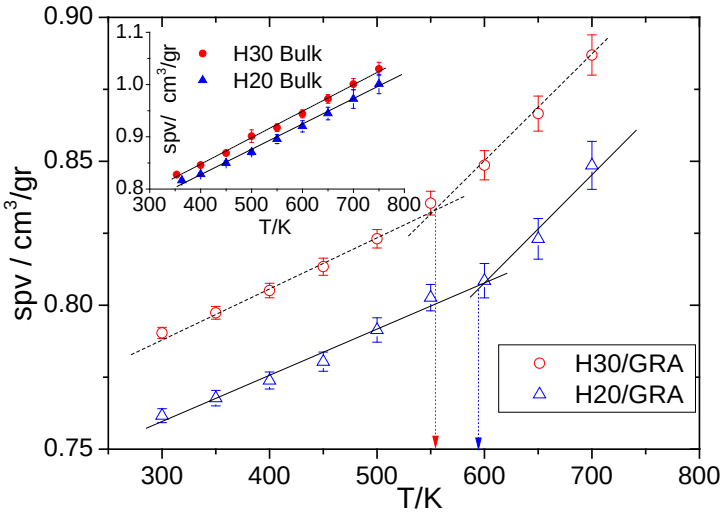

Figure 2: Temperature dependence of the specific volume of the examined nanocomposites (main panel, this work) and of the pristine polymers (inset, ref. [31]) . The dashed arrows in the main panel indicate the nominal temperatures corresponding to the changes in the slope of the curves.

For both systems a change in slope is observed in the temperature range between 550 K to 600 K indicating a glass-like transition[55]. Such a change in the corresponding picture characterizing the pristine polymer components in the melt state is absent at the examined temperature window as it is shown in figure 2 inset[31]. The experimentally-determined glass transition temperatures in the neat hyperbranched polyesters studied here, were found to be 30°C and 35°C for the H20 and the H30 respectively[56]. An alternative method for detecting changes in the thermal behavior of the systems is by monitoring their thermal expansion coefficient α_p. The latter can be calculated via the combined fluctuations of volume and enthalpy[57] as follows

$$\alpha_p = \frac{1}{K_B T^2 V}\left\langle \delta V \cdot \delta\left(K + P + PV\right)\right\rangle \quad (1)$$

In eq. 1, V denotes the volume, T the temperature, *K* the kinetic energy, *P* the potential energy, P the pressure and K_B the Boltzmann's constant. The so-calculated thermal expansion coefficient for the composite systems is illustrated in figure 3. A noticeable change in the behavior of α_p indicative of a sample undergoing a glass-like transition[58, 59], is observed at the same temperature range in which the changes in slope take place in figure 2.

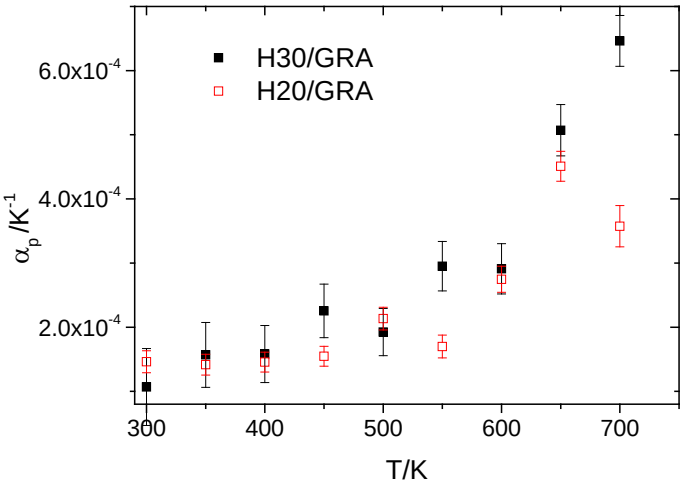

Figure 3: Temperature dependence of the thermal expansion coefficient of the composite systems upon cooling.

Although the absolute values of the detected glass-like transitions in figure 2 might have been affected by the relatively fast cooling rate of the simulations[60, 61] (here about $10^9 Ks^{-1}$), the temperature distance from the T_g values of the respective neat polymers attests to the different origin of the observed thermal transition in the composites. Monitoring of the energy variations as a function of temperature (see figure S1 in Supporting Information) showed no abrupt changes in the examined temperature range, in agreement with the behavior noted in polymer/carbon-nanotube composites[62].

Existence of a polymer-associated glass transition (T_g) at temperatures considerably higher compared to that of the pure polymer has been documented in several polymer/filler composites[63-66]. The origin of the shifted/high-temperature T_g was associated with a polymer layer of reduced mobility which was physically adsorbed on the filler's surface. In graphene-based polymer nanocomposites (including systems with graphite-oxide and/or chemically modified graphene) a shift of the T_g at higher

temperatures by several tens of degrees has been also observed even at very low content of the graphene-based material[15, 67]. In these studies it was found that the wrinkled morphology of the graphene flakes combined with the presence of functional groups, promoted the physical adsorption of the macromolecules onto the graphene sheets, enhancing thus the dynamic arrest of the interfacial polymeric chains and leading to an apparent shift of T_g at higher temperatures. This mechanism,however, is unlikely to be responsible for the manifestation of the high temperature T_g in our case, because of the relatively small size of the graphene flakes utilized. The nm-sized flakes used in this work do not favor the formation of sufficiently large wrinkles which could act as polymer-adsorption sites.

Recent computer simulation studies in systems comprised by linear polymers confined between two inflexible stationary graphene sheets[68-70], demonstrated that for polymers with different side groups along the polymer backbone and with a different level of the polymer/graphene attractive interactions, bonds belonging in the first layer adjacent to the graphene sheets assume slower reorientational mobility compared to the bulk, implying a higher glass transition temperature[71, 72].

Although the picture emerging from the aforementioned studies in linear polymer/graphene-based hybrids is compatible with an elevated (compared to the respective pristine polymers) glass transition temperature, some distinctions must be pointed out in the case where the soft component is a hyperbranched polymer, before any analogies can be drawn for our systems. Due to the strong connectivity constraints present in densely branched polymers (as in our case), the mechanisms responsible for the manifestation of glass-transition phenomena in such systems are more complex compared to their linear analogues[73-77]. For instance, in dendritic molecules a strong mobility contrast between monomers close to the topological center and those near the periphery[75, 78, 79] characterizes local motion, which (in case of high generation dendritic molecules) may even lead to the manifestation of multiple glass transitions[74, 76]. In this context, the high-temperature glass-like transition found in the examined composites will be discussed in conjunction with additional static and dynamic analysis in the sections to follow.

IV. Static/structural characterization of the systems

To obtain a detailed view of the structural features of the examined systems we have monitored the relative spatial arrangement of the two components in the mixture, as well as individual morphological characteristics which may affect the dynamic behavior and the mechanical response of the nanocomposites.

IV. 1. Morphological features of the hyperbranched molecules in the composite

To check for possible changes in the conformational characteristics at the lengthscale of the entire hyperbranched molecules in the presence of graphene, we have explored the average dimensions and the shape of the polymeric components as a function of temperature. Figure 4 compares the average radius of gyration of the polyesters in the composite and in the bulk in the examined temperature range. As shown, the average size of the polymers is only slightly lower in the composites (by approximately 5% to 7%).

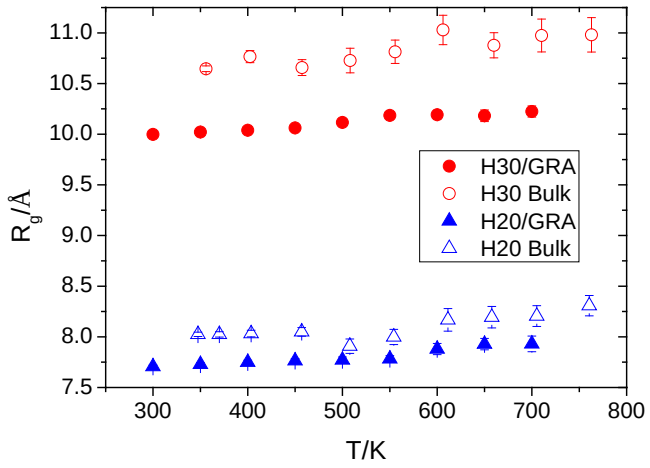

Figure 4: Temperature dependence of the average radius of gyration of the hyperbtanched polyesters in the composites and in the bulk.

To explore possible changes in the shape of the hyperbranched polyesters upon mixing them with graphene, we have compared the axes of the ellipsoid of inertia (see Supporting Information, figure S2) of the hyperbranched molecules in bulk and in hybrid systems as shown in figure 5.

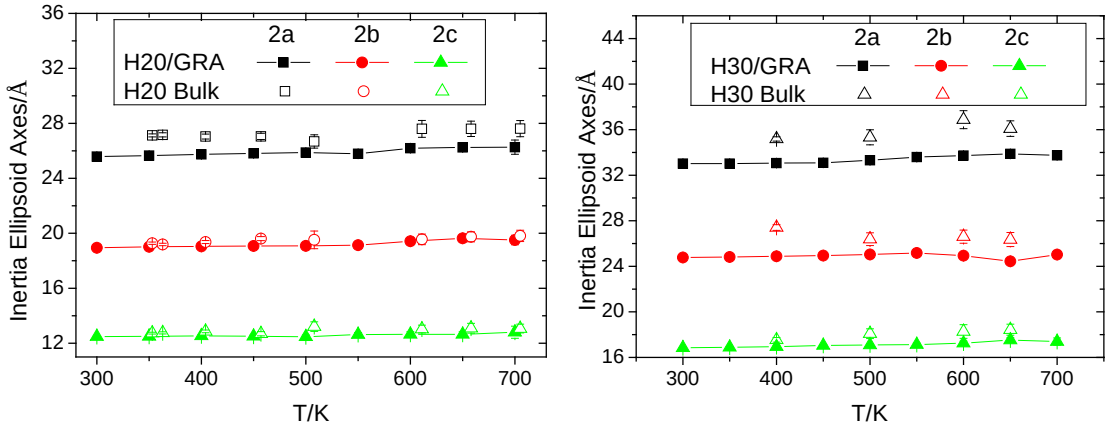

Figure 5. Axes of the ellipsoid of inertia of the hyperbranched polymers in the bulk (open symbols) and in the nanocomposite (filled symbols) at the examined temperatures. H20 systems are shown in the left and H30 systems in the right panel

According to the behavior described in figure 5, the shape of the polymeric components remains practically unaffected by the presence of graphene. Combining the results from figures 5 and 6, it appears that the hyperbranched molecules in the composites retain the morphological characteristics they assumed in the bulk state, even when each polymer resides in close contact with multiple graphene sheets (see fig. 1). This finding can be related to previous experimental efforts[80], where it was found that at high concentrations, near surfaces (i.e., at high surface coverage) hyperbranched polyesters similar to ours behave like regularly branched dendrimers in bulk, i.e., they retain almost their original shape, even in the case where the interactions with the surface are favorable and even if the generation of the molecules is kept low. This low deformability of the hyperbranched polymers near surfaces at high concentrations and/or in the absence of solvent, should essentially be associated with their dense connectivity pattern[81, 82] and furthermore for the hyperbranhced polyesters examined here with their tendency to form intra- and intermolecular hydrogen bonds[31, 83, 84] which stabilize their structure, enhancing thus the persistence of their morphological features.

IV. 2. Polymer density profiles

A common feature in polymer-based composite materials, is the formation of polymeric layers with distinct densities at different distances from the polymer/filler interface[85, 86]. Depending on the strength of the interactions between the polymeric matrix and the filler material and the severity of possible geometric constrictions, the pattern of the density profiles can be characterized by sharp and intense maxima close to the interface[86-88].

The density profiles of the hyperbranched polyesters along the direction perpendicular to the graphene planes as a function of the distance from the latter, are shown for the examined systems in figure 6.

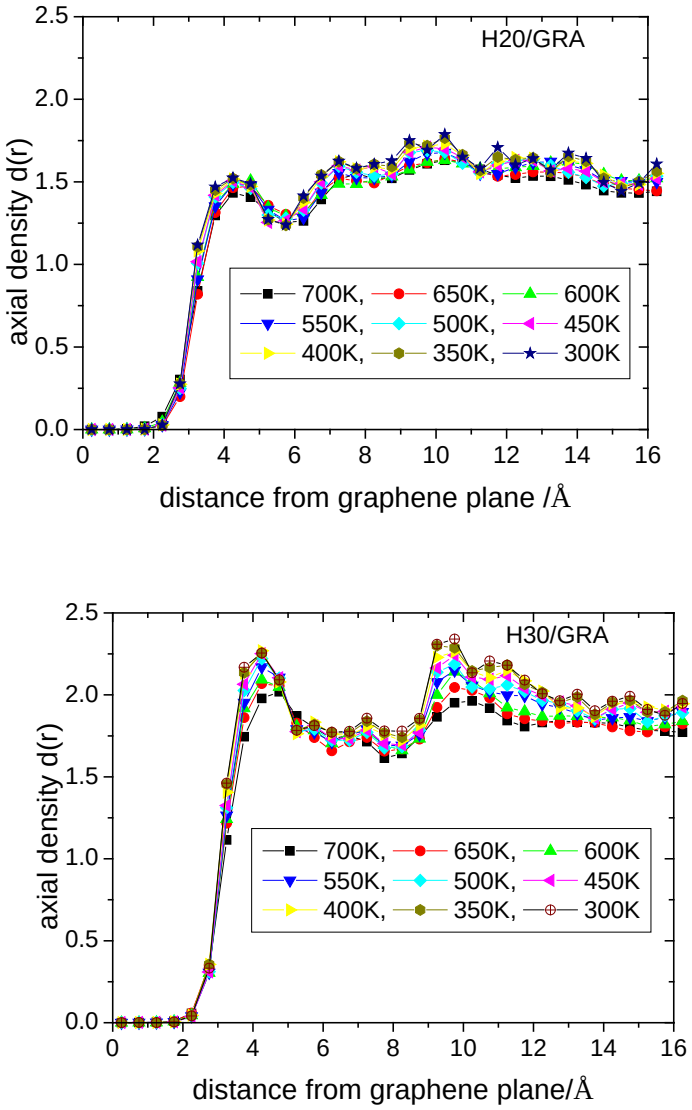

Figure 6 : Symmetrized axial density profiles of the polymeric components along the direction perpendicular to the graphene planes for the H20/GRA (upper) and the H30/GRA (lower panel) systems.

In the construction of these profiles no distinction was made between graphene sheets exposed to the polymer and those residing in-between other graphene flakes. In both systems a weak density modulation is observed which is rather insensitive to temperature variations. Differences between the location and the relative amplitude of the maxima can be noted when comparing the behavior in the two systems, with those characterizing the composite with the high molecular weight polyester being somewhat more intense. These disparities should be related to the discrete morphological characteristics of the H20 and the H30 molecules (see scheme 1) as well as to possible differences in the details of the graphene arrangement in the two systems . On one hand, the H30 polyester possesses a higher number of peripheral

bonds which may assume different packing behavior near graphene with respect to bonds located closer to the center of mass of the hyperbranched molecule. On the other hand H20 polyesters may assume more compact conformations due to the denser intramolecular hydrogen bonding network[31, 83, 84] which could affect the spatial arrangement of the bonds near the polymer/graphene interface.

When collating the features of the profiles of figures 6 with those characterizing linear polymers in graphene-based composites[69, 70] it becomes apparent that the intensity of the density peaks in our systems is much lower relative to the respective bulk values (in refs[68-70] the surface-adjacent density peaks reach 2 to 3 times the corresponding bulk values). Our results would better fit to profiles associated with a weak attractive interaction between the surface (here graphene) and the polymeric component[86]. This rather low density contrast between monomers close to graphene planes and those at larger distances in our systems, can already be taken as an indication that the origin of the high-temperature glass-like transition (section III) is unlikely to be related to an associated mobility contrast between these two populations of monomers.

IV. 3. Spatial arrangement of the graphene sheets in the composites

The details of the spatial arrangement of the filler in polymer nanocomposites is known to affect microscopically the dynamics of the polymeric matrix and macroscopically several of the physical properties of these materials[4, 33, 34]. To assess the details regarding the dispersion of the graphene in the polymeric matrix, we have examined the radial distribution function arising from the centers of mass of the graphene sheets through the entire temperature range. The corresponding spectra are presented in figure 7.

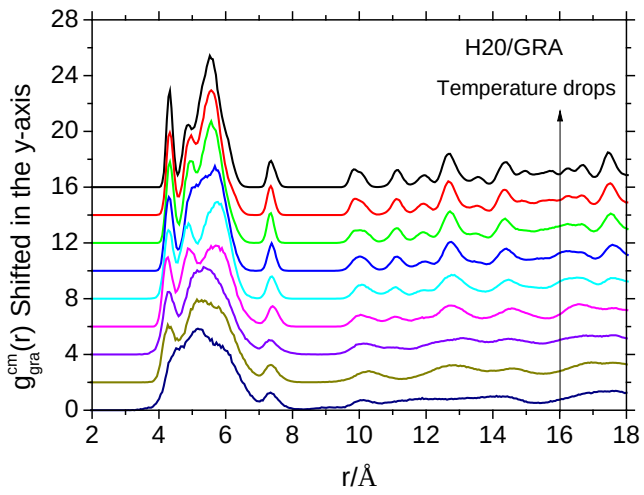

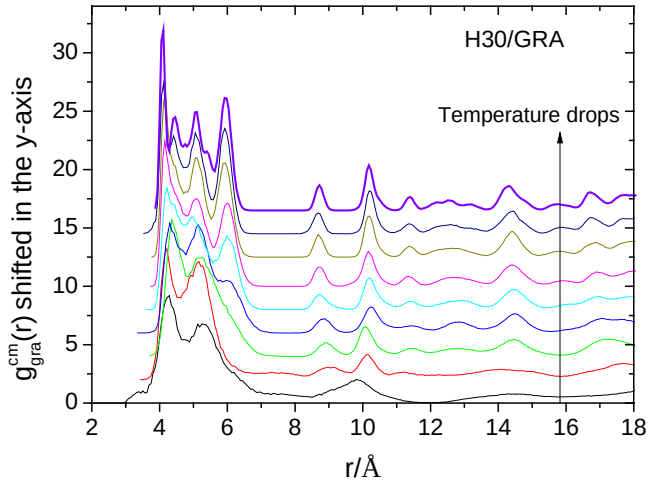

Figure 7: Radial distribution functions of the centers of mass of the graphene sheets for the H20/GRA (upper panel) and the H30/GRA (lower panel) systems, in the temperature range from 300K to 700K in 50K steps. The arrows denote the direction of temperature decrease. Each curve is shifted in the y-axis by a value of 2 with respect to the previous. The temperature with zero shift is 700K.

Following the curves as temperature drops, it can be observed that in both systems the high-temperature peaks grow sharper, while at temperatures lower than those identified as nominal glass transition temperatures (see figures 2 and 3) additional peaks appear. Both of these features imply the gradual consolidation of the graphene's spatial arrangement as temperature drops and the establishment of a structural order of the graphene planes. It is worth noticing the development of multiple peaks at short distances, which imply close neighboring (i.e., clustering) of graphene platelets. Moreover, the graphene clustering pattern seems to be affected by the size/topology of the polymeric component.

To further elaborate on the arrangement of graphene in the composite, we have calculated the orientational order parameter of the graphene planes, according to eq. 2.

$$P_2(\theta) = \frac{1}{2}\left\langle 3\cos^2\theta - 1 \right\rangle \qquad (2)$$

In eq. 2, θ denotes the angle between the vectors perpendicular to two graphene planes and the angle brackets indicate an ensemble and time average. A value of $P_2(\theta)$ equal to 1 would indicate parallel orientation of the planes, a value of -0.5 a perpendicular arrangement and a value of 0 a random orientation.

Figure 8 depicts the dependence of the aforementioned order parameter on the distance between the centers of mass of neighboring graphene platelets in the entire temperature range.

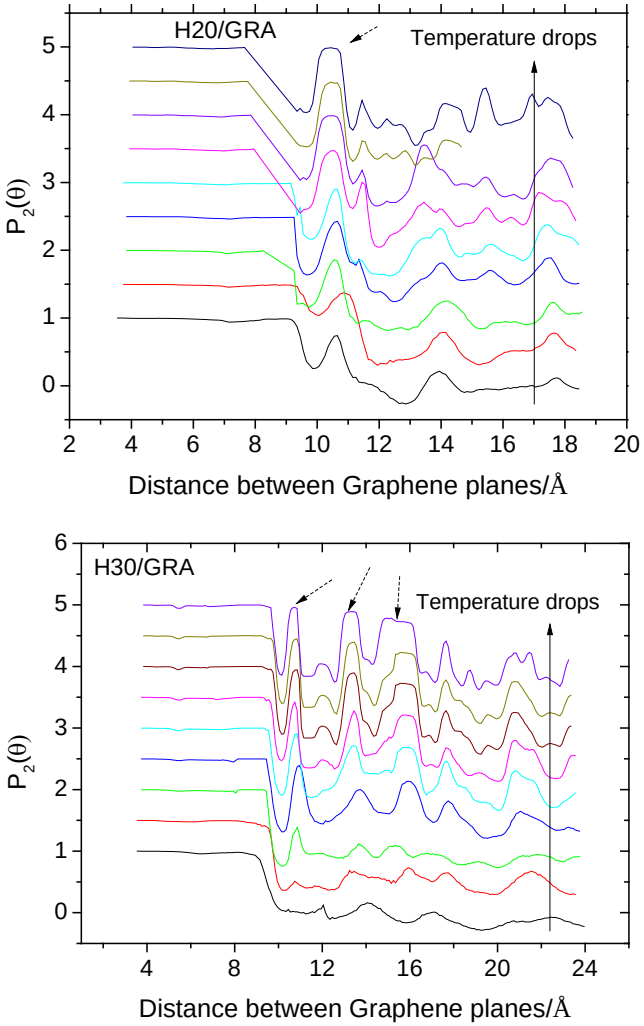

Figure 8: Orientational order parameter of the graphene planes for the H20/GRA (upper panel) and the H30/GRA (lower panel) systems, in the temperature range from 300K to 700K in 50K steps. The solid arrows denote the direction of temperature drop. The dashed arrows indicate areas of almost parallel orientation at larger distances. Each curve is shifted in the y-axis by a value of 0.5 with respect to the previous. The temperature with zero shift is 700K.

A common feature shared by the two systems is that at distances below 8-9Å a parallel orientation of immediately neighboring graphene planes is realized. In addition, as temperature decreases, orientational peaks corresponding to an almost parallel arrangement are also developing at larger graphene separations (dashed arrows in figure 8). Such areas are more frequent in the system with the higher in size hyperbranched polyester (H30/GRA). The parallel orientation at short distances is

consistent with the formation of bundles comprised by stacked graphene flakes, while values of the order parameter close to 1 at larger distances could arise by an almost parallel orientation of neighboring individual graphene flakes or multi-platelet graphene layers.

The tendency of graphene platelets to stack in layers is known, but the characteristics of the formed layers differ depending on the thermodynamic microenvironment [89-91]. The details of the graphene dispersion may actually play a significant role in the physical properties of the resulting composite materials[35, 90]. To complement the picture emerged by analysis of the spatial arrangement of graphene in the polymeric matrix (figures 7,8), we have examined relevant simulations snapshots, as illustrated in figure 9.

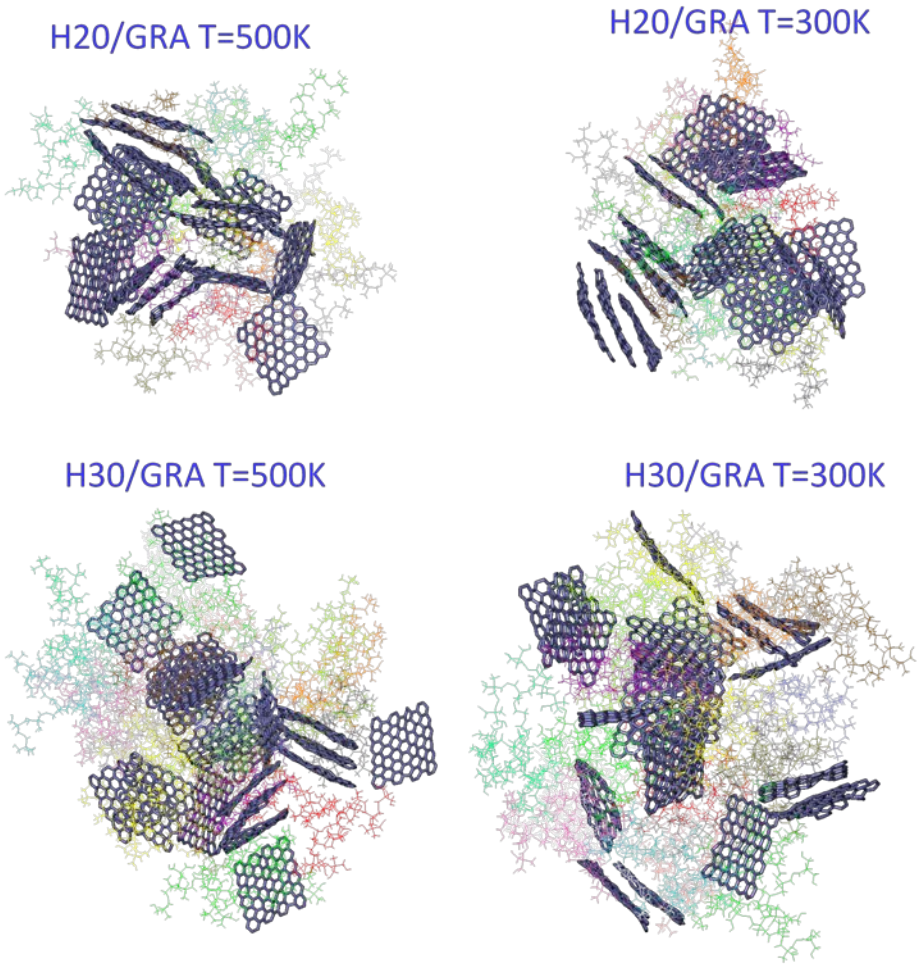

Figure 9: Snapshots of the examined systems at two temperatures. Each hyperbranched molecule appears with a different color for clarity.

Inspection of the snapshots attests to the existence of individual (i.e., exfoliated) graphene platelets as well as the formation of graphene layers comprised by 2 to 3

stacked flakes and the existence of neighboring such clusters with similar orientation, as was deducted from figures 7 and 8.

V. Dynamic properties of the polymeric components

The freezing-in of the graphene-related structure upon temperature decrease as described above, essentially creates a fixed geometry which is expected to affect significantly the dynamic response of the polymer molecules. To examine such effects, we have explored characteristic motional processes related to local as well as to the entire molecular scale of the hyperbranched polyesters.

V.1 Local bond reorientation

To examine dynamics in a local lengthscale, we have monitored the reorientational motion of the carbon-carbon bonds (CT-CT) belonging to a branch and of the carbon-hydroxyl oxygen (CT-OH) bonds (see scheme 1). This selection is based on the different degree of motional freedom expected for the two kinds of bonds. To probe the bonds' motion we have calculated the second order orientational correlation function according to eq. 3

$$C(t) = \frac{1}{2}\left\langle 3\left[\hat{h}(t)\cdot\hat{h}(0)\right]^2 - 1\right\rangle \qquad (3)$$

where $\hat{h}(t)$ represents a unit vector along the examined bond at time t. Figure 10 depicts such orientational correlation functions for the examined bonds in the composite systems and compares them with those corresponding to the neat polymers[31]. For both the examined bonds and for both the composite systems, spectra describing the latter (solid lines) appear to decorrelate at longer timescales compared to those describing bulk polymers (symbols) at similar temperatures. Analysis of the presented spectra has been performed by means of the calculation of the distribution of exponential relaxation times (DRT)[92, 93] according to eq. 4

$$C(t) = \int_{-\infty}^{\infty} F(\ln\tau)\, e^{-t/\tau}\, d\ln\tau \qquad (4)$$

In this notation, each correlation function is described as a continuous superposition of single exponential processes with a probability distribution $F(\ln\tau)$. In eq. 4 τ

symbolizes a characteristic exponential relaxation time. A distinct peak in the distribution spectra denotes a separate motional process characterized by its most probable relaxation time (to a first approximation the location of the maximum), its width, associated with local dynamic heterogeneity close to that timescale, and its total amplitude (the area under the peak) denoting the relative contribution of this process to the overall decay of the examined correlation function. For instance, dynamic processes such as the rapid tumbling motion of a bond, its local rotational motion, the reorientation of the branch in which the bond belongs or even the reorientation of the entire molecule may appear as distinct processes in the bond DRT spectra if their timescales are sufficiently separated[31, 94] The first moment of the distribution in τ, corresponds to an average relaxation time, taking into account all partial relaxational mechanisms as described above. Such distributions are shown as an example in figure 11 for systems containing the higher generation hyperbranched polyester (H30, H30/GRA).

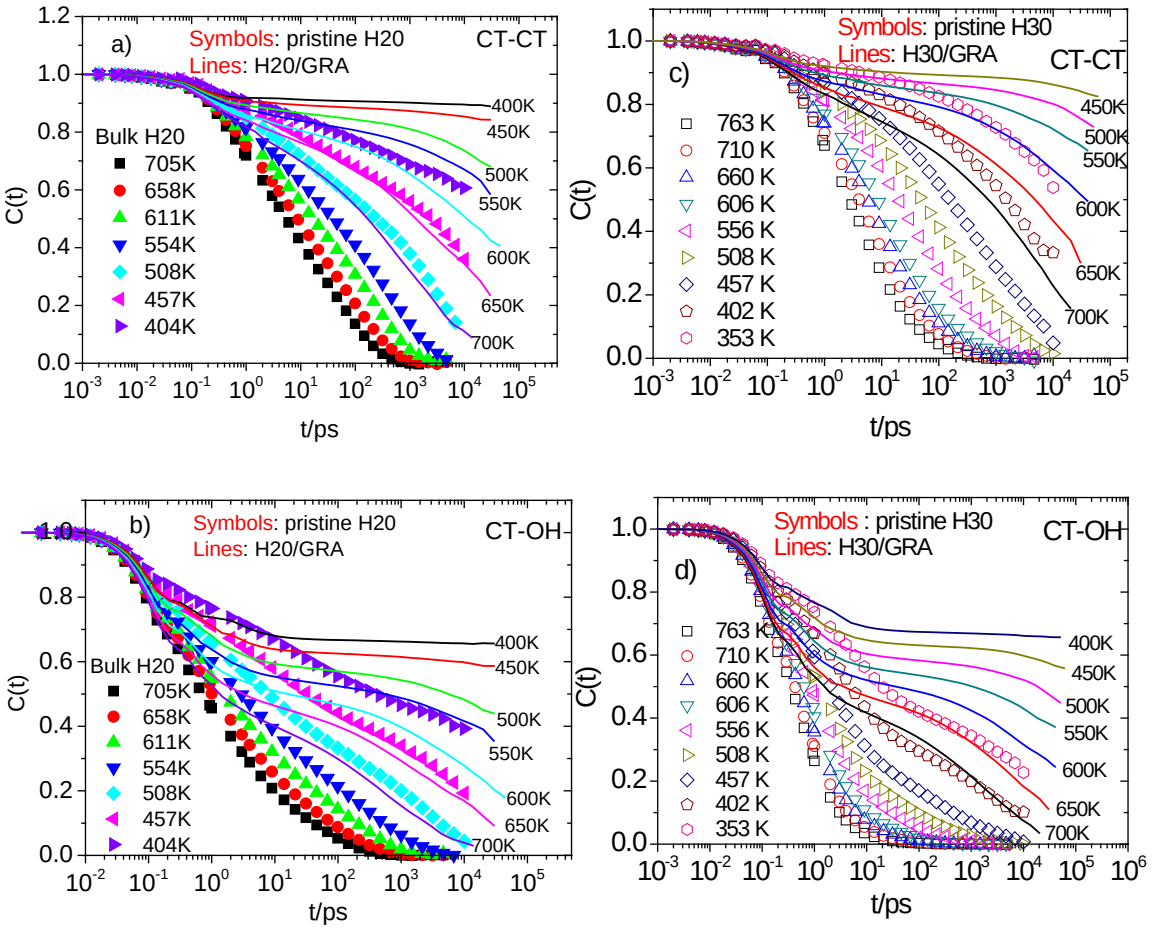

Figure 10 : Orientational correlation functions for the carbon-carbon (a,c) and the carbon-oxygen (b,d) bonds of the H20 (a,b) and the H30 (c,d) based systems. Spectra for the pristine polymers are taken from ref. [31].

Since we are examining local dynamics which is closely associated with glass transition phenomena, we have compared distributions at temperatures equidistant from their nominal glass transitions (for the composite system we have considered the Tg value identified in figure 2 and for the pristine system the experimentally measured value), so that they would correspond to similar mobility states (comparison at similar temperatures are provided in Supporting Information, figure S3).. Visual inspection of the DRTs in figure 11 shows that for both kinds of the examined bonds, there exist clear differences between the behavior of the neat polymer and that of the polymer in the composite. The differences observed in the spectral features of each peak (location of the maximum, shape, width) indicate that the examined bonds in the composite and in the bulk experience distinct microenvironments as far as it concerns their motional freedom.

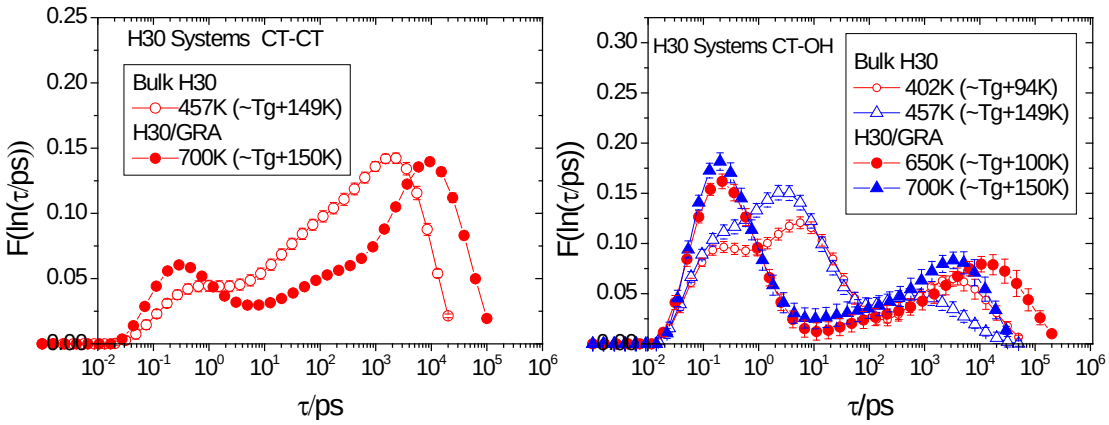

Figure 11: Comparison of distributions of relaxation times from the analysis of the reorientational correlation functions for the carbon-carbon (left) and the carbon-oxygen (right) bonds from the H30-based systems. Error bars are shown only if they exceed the size of the symbols.

To quantify the observed differences in terms of the timescale pertinent to the examined motion, we have calculated the average relaxation times corresponding to the correlation functions shown in figure 10 based on their DRT analysis and mapped their temperature dependence as portrayed in figure 12. It should be noted that in this plot, relaxation times appear only for temperatures at which there is a sufficient degree of decorrelation so that the DRT analysis can be performed in a reliable manner.

The first characteristic that can be noticed when comparing the behavior in the absence and in the presence of graphene, is that the relaxation rates in the composite are much lower (i.e., the reorientational times are much longer). A second observation is that it appears that the temperature dependence of the relaxation rates is much stronger in hybrid systems, indicating that in this case local dynamics of hyperbranched molecules become more cooperative in nature[95, 96]. In addition, it appears that the presence of graphene has altered the relative contrast in reorientational mobility between the carbon-carbon and the carbon-oxygen bonds in the H20/GRA system with respect to the bulk. This might be related to more significant changes in the hydrogen bonding network of the H20 component, which could affect local dynamics of the hydroxyl oxygen[31].

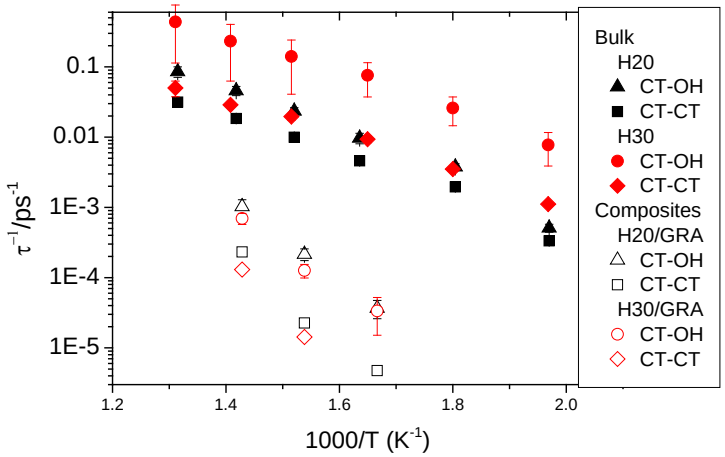

Figure 12: Average relaxation rates as a function of inverse temperature for the carbon-carbon (CT-CT) and the carbon-oxygen (CT-OH) bond correlation functions appearing in figure 10. Error bars are shown if their size exceeds that of the symbols.

V.2 Dynamics at the entire molecular scale

Given the enhanced coupling of short lengthscale motions with the size and the conformational characteristics related to the entire molecular scale in dendritic polymers[78, 94] and more specifically in the examined hyperbranched polyesters due to their extensive hydrogen bonding capabilities[31, 56, 84, 97], study of global polymer dynamics is of particular interest in our systems.

To examine dynamics in the molecular scale, we have calculated self-correlation functions $G_v(t)$ analogous to those described by eq. 3, but this time $\hat{h}(t)$ refers to unit vectors along directions pointing from the center of mass of a hyperbranched

polymer to individual monomers throughout the entire structure. The latter functions essentially probe the rotational motion of the entire polymer. Figure 13 displays $G_v(t)$ for the neat polymers and those in the composites at different temperatures. Evidently, the degree of decorrelation of the functions describing the motion of the polyesters in the nanocomposites is considerably lower when compared to those of the neat polymers in the melt at similar temperatures. In other words, global rotational motion is much slower in the presence of graphene. Moreover, the degree of slowing-down in polymer motion in the two composites depends on the size of the polymeric component. The larger the size, the larger the degree of retardation.

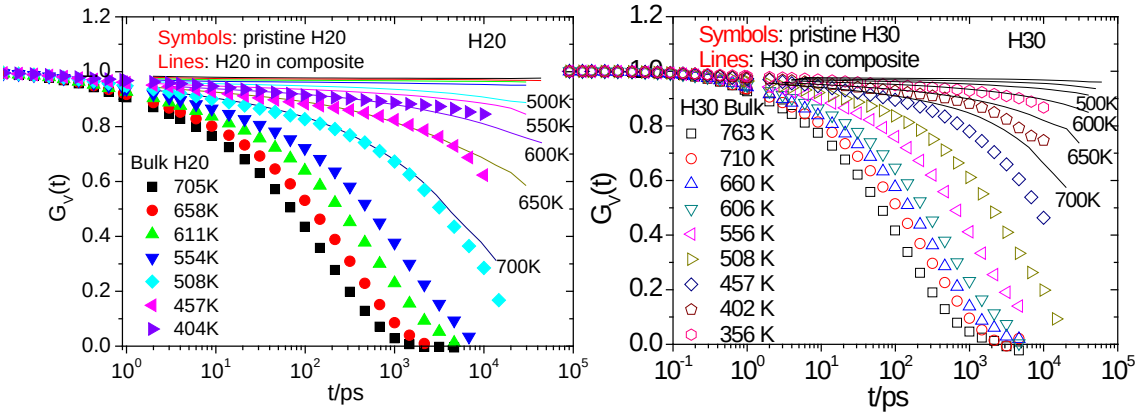

Figure 13: Comparison of the rotational relaxation functions $G_v(t)$ between the neat hyperbranched polymers (symbols) and those in the composite systems (lines). The arithmetic labels attached to the latter denote the corresponding temperatures.

To calculate average relaxation times corresponding to relaxation functions shown in figure 13, we resorted to a different procedure due to the rather low degree of decorrelation of most of the respective correlation curves. This method was based on the estimation of the temperature shift factors necessary for the respective correlation functions to superpose in a single mastercurve. We present this procedure for the H20/GRA system in which the degree of decay of the respective correlation functions is higher. For the polymeric component of this system in its pristine melt state, relevant experimental measurements (see figures S4 and S5 in Supporting Information) showed that to a good approximation time-temperature superposition holds. The results of this procedure are depicted in figure 14.

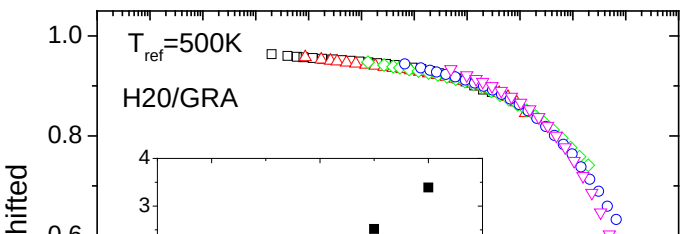

Figure 14: Rotational relaxation functions for the H20/GRA systems shifted as described in the text, using as reference temperature T_{ref}=500K. The inset shows the resulted shift factors as a function of temperature.

By calculating the average relaxation time corresponding to 700K (where the degree of decorrelation is sufficiently progressed) via the DRT analysis and using for the other temperatures the shift factors resulted from the procedure described above (figure 14 inset), we were able to estimate the respective relaxation times for lower temperatures as well. The so-estimated relaxation rates of the H20/GRA system together with those corresponding to the neat polymers, are plotted in figure 15.

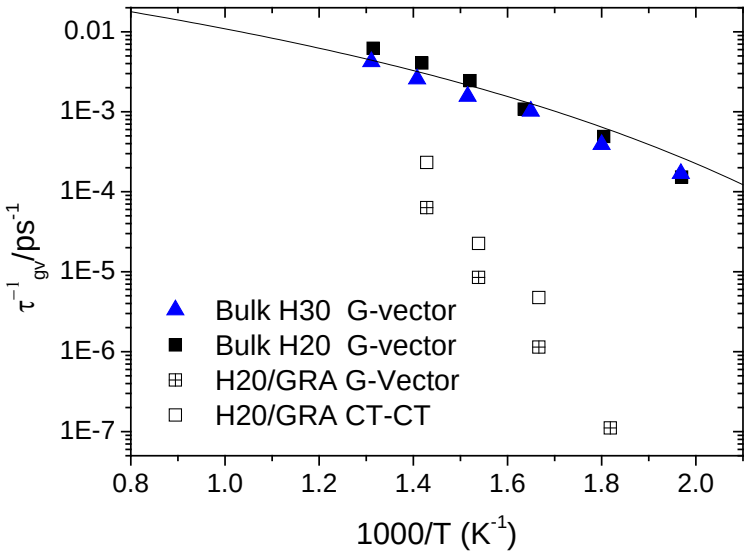

Figure 15: Average relaxation rates for the global rotational motion of the neat polymers (from ref. [31]) and of the H20/GRA system. Points corresponding to CT-CT bond orientational dynamics are also repeated from figure 12 for comparison purposes. The line represents the temperature dependence of the experimentally determined rheological shift factors for the pristine H20 melt (see figure S5 in Supporting Information).

Apparently the relaxation rates describing the composite system are several orders of magnitude lower compared to those of the neat polymers, while they also exhibit a stronger temperature dependence indicating a differentiation in the mechanism of global rotation between the composite and the bulk. Although we expect that this relaxation would have borne the characteristics of a Williams-Landel-Ferry[98] process had the lower temperatures been accessible to the simulation, based on the high temperature behavior shown in fig. 15 we can calculate an effective activation energy of 32.1±0.9 kcal/mol, which is rather high and reflects the hindered nature of this motion. If we attempt to apply the same shifting procedure for the H30/GRA system as well (see figures S6 and S7 in Supporting Information), the resulting shift factors exhibit the same temperature dependence with those describing the H20/GRA system indicating that a similar relaxational mechanism characterizes polymer motion in the entire molecular scale in both composites.

V.3 Association of polymer dynamics with the high-temperature T_g

According to the previous sections describing dynamic properties, the presence of graphene imparts a significant slowing-down of polymer dynamics, both, in local and in global scale. A question, thus, arises as to which is the key mechanism responsible for the manifestation of the high temperature T_g.

As has been mentioned earlier, in the case where a slowing down of local dynamics in linear polymer was observed near the polymer/filler interface (which can be associated with an elevation of T_g with respect to the neat polymer[99]), this was associated[70, 86, 88] with the formation of a physically adsorbed polymer layer with significantly increased density compared to bulk values. In our case, the excess polymer density (with respect to the bulk) observed near to the graphene/polymer interface is very low compared to those detected for linear polymer composites as discussed in section V.2 and therefore it is quite unlikely that this could account for the dramatic slowing-down by 2 to 3 orders of magnitude of local motion shown in Fig. 12.

On the other hand, previous studies have demonstrated that the influence of the global dynamics to local motion in polymers bearing dendritic structure, becomes increasingly important as the degree of retardation in the entire molecular scale motion increases[78, 100]. In particular, the slow motional process which appears in local

dynamics in dendritic polymers (in high molecular weights more than one such processes may appear[74, 78]) and which was shown to be directly related to global motion, can become the dominant relaxational channel for local bond reorientation[78] when the slowing-down of global motion increases significantly. The resemblance of this slow process in terms of its relaxation time and its temperature dependence with that describing the global polymer rotational motion has been demonstrated in the pristine H20 and H30 systems[31]; it is also demonstrated in Fig. 15 by noting the proximity in timescale and the resemblance in temperature dependence between the rates describing global rotational motion and bond reorientation in the composites. Actually, the DRT spectra through which the average relaxation rates depicted in figure 12 were calculated, are dominated by the slow process (see Fig. 11 and Fig. S3 in the Supporting Information).

The strong association of this slow mode in local dynamics of hyperbranched polymers with dynamics in the entire molecular scale, arises from the fact that in such molecules complete reorientation of the bonds not far from the topological centers is realized only if the orientational relaxation of the entire molecule has been realized as well. In high molecular weight dendritic polymers where the percentage of such bonds is significant and the mobility contrast between them and those with accessibility to the periphery is high, more than one glass transition can be observed as quoted earlier. The low-temperature glass transition is essentially associated with the bonds experiencing a higher degree of motional freedom while the higher-temperature glass transition with the more constricted bonds which lie deeper within the dendritic structure, because of the much longer timescale required for the reorientation of the entire molecule.[74] In the present case of rather low generation branched polymers, the mechanism associated with the manifestation of a high temperature glass transition is absent in the pristine polymers (see ref [31] and inset of figure 2), while the low-temperature glass transition would lie at temperatures below the examined range. It is therefore reasonable to visualize that in the composite systems the much slower global polymer reorientational motion induced by the presence of graphene, can be considered responsible for the manifestation of the higher-temperature glass transition via a mechanism analogous to that giving rise to the high temperature Tg in larger generation dendritic molecules, by means of the obstruction of global reorientation of the hyperbranched polyesters, as described above.

VI. Summary/Conclusions

The main purpose of the present study was to obtain a deeper insight on the microscopic mechanisms which are involved in the manifestation of physical phenomena in systems comprised by multifunctional soft-colloidal compounds, such as hyperbranched polymers, and a very promising filler material with unique properties, such as graphene[14]. We have selected a particular category of hyperbranched polymers, that of hydroxyl-terminated polyesters, due to their low cost, their wide commercial availability and the previous knowledge on their physical behavior down to the microscopic scale[12, 31, 97, 101] .

Our results showed that at the examined volume fractions, graphene flakes can be present as individual platelets but at most they appear to organize in stacks (figure 8) comprised by 2 to 3 flakes (figures 1,9). The presence of graphene dimers and trimers has been correlated with maximization of the composite modulus as a function of the number of graphene flakes in previous studies[35, 90], which in combination with the lower viscosity characterizing the hyperbranched molecules and their thermal stability, render such hybrids ideal candidates for optimization of mechanical response and processability.

As the temperature lowers, the gradual consolidation of the graphene-related structure constricts the global polymer motion resulting in a significant slowing down compared to their behavior in the melt (figures 13, 15). However, the average size and shape of the hyperbranched molecules practically are not affected (figures 4,5) and their density profiles exhibit only a weak modulation as a function of the distance from the graphene planes (figure 6). This should be contrasted to the tendency of linear polymers to assume almost planar conformations and to exhibit sharp density fluctuations near surfaces in the glassy state, even if the interactions with the surface are non-attractive[85].

This geometrically-hindered global molecular motion (but without any appreciable change in the polymer dimensions) appears to affect drastically local scale dynamics as well (figures 10,11,12). Such an effect is not necessarily expected in linear polymers[102] and it should be attributed to the close interconnection between local and global dynamics in dendritic polymers due to the strong connectivity constraints imposed by the dense branching pattern[74, 78].

Although in the present work we examined composites of graphene with a specific category of hyperbranched polymers, several aspects of the observed behavior were associated with generic properties of the two components. Therefore, we believe that comprehension of the behavior of the examined systems may serve as a starting point for a better understanding of nanocomposite materials involving graphene and highly branched polymers in a more general sense.

Supporting Information

Energy contributions as a function of temperature, definition of the ellipsoid of inertia, comparison of the distributions of relaxations times arising from analysis of orientational correlation functions of the CT-CT and the CT-OH bonds, time temperature superposition for rheological measurement of H20, and time-temperature shift of the Gv times for the H30/GRA system

This material is available free of charge via the Internet at http://pubs.acs.org.

Acknowledgments

This research has been co-financed by the European Union (European Social Fund – ESF) and Greek national funds through the Operational Program "Education and Lifelong Learning" of the National Strategic Reference Framework (NSRF) - Research Funding Program: Thales. Investing in knowledge society through the European Social Fund (MIS 377278).

REFERENCES

1. Beall, G. W.; Powell, C. E., *Fundamentals of Polymer–Clay Nanocomposites*. Cambridge University Press: Cambridge, UK, 2011.
2. Vilgis, T.; Heinrich, G.; Klüppel, M., Reinforcing fillers. In *Reinforcement of Polymer Nanocomposites*, Cambridge University Press: 2009; p 75.
3. Mittal, V., *Polymer Nanotube Nanocomposites*. John Wiley & Sons, Inc.: Hoboken, New Jersey, 2010.
4. Mukhopadhyay, P.; Gupta, R. K., *Graphite, Graphene, and their polymer nanocomposites*. CRC Press: 2013.
5. Soler-Illia, G. J. A. A.; Azzaroni, O. *Chemical Society Reviews* **2011,** 40, 1107-1150.
6. Konwar, U.; Karak, N. *Polym J* **2011,** 43, 565-576.
7. Amin, A.; Samy, M. *Int. J. Polym. Sci.* **2013,** 2013, 528468,.
8. Santra, S.; Kaittanis, C.; Perez, J. M. *Langmuir* **2009,** 26, 5364-5373.
9. Uhrich, K. E.; Hawker, C. J.; Frechet, J. M. J.; Turner, S. R. *Macromolecules* **1992,** 25, 4583-4587.
10. Frechet, J. M. J. *Science* **1994,** 263, 1710.
11. Gao, C.; Yan, D. *Prog. Polym. Sci.* **2004,** 29, 183-275.
12. Malmström, E.; Johansson, M.; Hult, A. *Macromolecules* **1995,** 28, 1698-1703.
13. Perstorp http://www.perstorp.com/
14. Geim, A. K.; Novoselov, K. S. *Nat Mater* **2007,** 6, 183-191.
15. RamanathanT; Abdala, A. A.; StankovichS; Dikin, D. A.; Herrera Alonso, M.; Piner, R. D.; Adamson, D. H.; Schniepp, H. C.; ChenX; Ruoff, R. S.; Nguyen, S. T.; Aksay, I. A.; Prud'Homme, R. K.; Brinson, L. C. *Nat Nano* **2008,** 3, 327-331.
16. Decker, J. J.; Chvalun, S. N.; Nazarenko, S. *Polymer* **2011,** 52, 3943-3955.
17. Rodlert, M.; Plummer, C. J. G.; Grunbauer, H. J. M.; Manson, J. E. *Adv. Eng. Mater.* **2004,** 6, 715-719.
18. Rodlert, M.; Plummer, C. J. G.; Garamszegi, L.; Leterrier, Y.; Grunbauer, H. J. M.; Manson, J.-A. E. *Polymer* **2004,** 45, 949-960.

19. Luciani, A.; Plummer, C. J. G.; Nguyen, T.; Garamszegi, L.; Manson, J. A. E. *J. Polym. Sci. Pt. B-Polym. Phys.* **2004,** 42, 1218-1225.
20. Plummer, C. J. G.; Garamszegi, L.; Leterrier, Y.; Rodlert, M.; Manson, J. A. E. *Chem. Mater.* **2002,** 14, 486-488.
21. Fogelström, L.; Antoni, P.; Malmström, E.; Hult, A. *Progr. Org. Coating.* **2006,** 55, 284-290.
22. Fogelström, L.; Malmström, E.; Johansson, M.; Hult, A. *ACS Appl. Mater. Inter.* **2010,** 2, 1679-1684.
23. Zhu, J.; Zhang, H.; Kotov, N. A. *ACS Nano* **2013,** 7, 4818-4829.
24. Zhang, Q. H.; Zhao, X.; Chen, D. J.; Lu, P. *Macromolecules* **2010,** 43, 2357-2363.
25. Zaman, I.; Kuan, H. C.; Meng, Q. S.; Michelmore, A.; Kawashima, N.; Pitt, T.; Zhang, L. Q.; Gouda, S.; Luong, L.; Ma, J. *Adv. Funct. Mater.* **2012,** 22, 2735-2743.
26. Yoonessi, M.; Gaier, J. R. *Acs Nano* **2010,** 4, 7211-7220.
27. Vickery, J. L.; Patil, A. J.; Mann, S. *Adv. Mater.* **2009,** 21, 2180-2184.
28. Konatham, D.; Bui, K. N. D.; Papavassiliou, D. V.; Striolo, A. *Mol Phys* **2011,** 109, 97-111.
29. Papavassiliou, D. V.; Bui, K.; Duong, H. M.; Striolo, A. *J Phys Chem C* **2011,** 115, 3872-3880.
30. Shau, S. M.; Juang, T. Y.; Lin, H. S.; Huang, C. L.; Hsieh, C. F.; Wu, J. Y.; Jeng, R. J. *Polym Chem-Uk* **2012,** 3, 1249-1259.
31. Tanis, I.; Karatasos, K. *Macromolecules* **2009,** 42, 9581.
32. Li, H.; Han, L.; Cooper-White, J. J.; Kim, I. *Nanoscale* **2012,** 4, 1355-1361.
33. Scocchi, G.; Posocco, P.; Fermeglia, M.; Pricl, S. *J Phys Chem B* **2007,** 111, 2143-2151.
34. Fotiadou, S.; Karageorgaki, C.; Chrissopoulou, K.; Karatasos, K.; Tanis, I.; Tragoudaras, D.; Frick, B.; Anastasiadis, S. H. *Macromolecules* **2013,** 46, 2842-2855.
35. Gong, L.; Young, R. J.; Kinloch, I. A.; Riaz, I.; Jalil, R.; Novoselov, K. S. *ACS Nano* **2012,** 6, 2086-2095.
36. Guo, S.; Dong, S. *Chemical Society Reviews* **2011,** 40, 2644-2672.
37. Weiner, S. J.; Kollman, P. A.; Nguyen, D. T.; Case, D. A. *J Comput Chem* **1986,** 7, 230-252.
38. Tsai, J. L.; Tzeng, S. H.; Tzou, Y. J. *Int J Solids Struct* **2010,** 47, 503-509.
39. Tsai, J. L.; Tu, J. F. *Mater Design* **2010,** 31, 194-199.
40. Scarpa, F.; Adhikari, S.; Phani, A. S. *Nanotechnology* **2009,** 20, 065709.
41. Zhao, X. C. *J Phys Chem C* **2011,** 115, 6181-6189.
42. Lv, W. P.; Chen, M. D.; Wu, R. A. *Soft Matter* **2013,** 9, 960-966.
43. Katoch, J.; Kim, S. N.; Kuang, Z. F.; Farmer, B. L.; Nalk, R. R.; Tatulian, S. A.; Ishigami, M. *Nano Lett.* **2012,** 12, 2342-2346.
44. Martínez, L.; Andrade, R.; Birgin, E. G.; Martínez, J. M. *J Comput Chem* **2009,** 30, 2157-2164.
45. Bellido, E. P.; Seminario, J. M. *J. Phys. Chem. C* **2010,** 114, 22472–22477.
46. Feller, S. E.; Zhang, Y.; Pastor, R. W.; Brooks, B. R. *J Chem Phys* **1995,** 103, 4613-4621.
47. Darden, T.; Perera, L.; Li, L.; Pedersen, L. *Structure* **1999,** 7, R55-R60.
48. Phillips, J.; Braun, R.; Wang, W.; Gumbart , J.; Tajkhorshid, E.; Villa, E.; Chipot, C.; Skeel, R.; Kale, L.; Schulten, K. *J. Comput. Chem.* **2005,** 26, 1781–1782.
49. Zhang, T.; Xue, Q. Z.; Zhang, S.; Dong, M. D. *Nano Today* **2012,** 7, 180-200.
50. Fasolino, A.; Los, J. H.; Katsnelson, M. I. *Nat Mater* **2007,** 6, 858-861.

51. Meyer, J. C.; Geim, A. K.; Katsnelson, M. I.; Novoselov, K. S.; Booth, T. J.; Roth, S. *Nature* **2007,** 446, 60-63.
52. Ishigami, M.; Chen, J. H.; Cullen, W. G.; Fuhrer, M. S.; Williams, E. D. *Nano Lett.* **2007,** 7, 1643-1648.
53. Menczel, J. D.; Prime, R. B., *Thermal Analysis of Polymers. Fundamentals and Applications*. John Wiley & Sons, Inc.: Hoboken, New Jersey, 2009.
54. Mark, J.; Ngai, K.; Graessley, W.; Mandelkern, L.; Samulski, E.; Koenig, J.; Wignall, G., *Physical Properties of Polymers*. Cambridge University Press: Cambridge, United Kingdom, 2004.
55. Paul, W., Determining the Glass Transition in Polymer Melts. In *Reviews in Computational Chemistry*, John Wiley & Sons, Inc.: 2007; pp 1-66.
56. Zhu, P. W.; Zheng, S.; Simon, G. *Macromol. Chem. Phys.* **2001,** 202, 3008-3017.
57. Lagache, M.; Ungerer, P.; Boutin, A.; Fuchs, A. H. *Phys. Chem. Chem. Phys.* **2001,** 3, 4333-4339.
58. Bicerano, J., *Prediction of Polymer Properties*. Marcel Dekker Inc: New York, 2002.
59. Niss, K.; Gundermann, D.; Christensen, T.; Dyre, J. C. *Phys. Rev. E.* **2012,** 85, 041501.
60. Torres, J. A.; Nealey, P. F.; de Pablo, J. J. *Phys. Rev. Lett.* **2000,** 85, 3221-3224.
61. Lucyshyn, T.; Knapp, G.; Kipperer, M.; Holzer, C. *J Appl Polymer Sci* **2012,** 123, 1162-1168.
62. Jiang, C.; Zhang, J.; Lin, S.; Jiang, D. *J Chem Eng Mater Sci* **2014,** 2, 26-30.
63. Tsagaropoulos, G.; Eisenburg, A. *Macromolecules* **1995,** 28, 396-398.
64. Chen, L.; Zheng, K.; Tian, X.; Hu, K.; Wang, R.; Liu, C.; Li, Y.; Cui, P. *Macromolecules* **2009,** 43, 1076-1082.
65. Robertson, C. G.; Rackaitis, M. *Macromolecules* **2011,** 44, 1177-1181.
66. Li, L.; Zhou, D.; Huang, D.; Xue, G. *Macromolecules* **2013,** 47, 297-303.
67. Xue, Q.; Lv, C.; Shan, M.; Zhang, H.; Ling, C.; Zhou, X.; Jiao, Z. *Comput. Mater. Sci.* **2013,** 71, 66-71.
68. Rissanou, A.; Harmandaris, V. *J Nanopart Res* **2013,** 15, 1-14.
69. Rissanou, A. N.; Harmandaris, V. *Macromol. Symp.* **2013,** 331-332, 43-49.
70. Rissanou, A. N.; Harmandaris, V. *Soft Matter* **2014,** 10, 2876-2888.
71. Priestley, R. D.; Broadbelt, L. J.; Torkelson, J. M.; Fukao, K. *Phys. Rev. E* **2007,** 75, 061806.
72. Ngai, K., The glass transition and the glassy state. In *Physical Properties of Polymers*, Cambridge University Press: 2004; p 72.
73. Karatasos, K. *Macromolecules* **2005,** 38, 4472-4483.
74. Karatasos, K. *Macromolecules* **2006,** 39, 4619.
75. Karatasos, K.; Lyulin, A. V. *J. Chem. Phys.* **2006,** 125, 184907.
76. Smirnova, N. N.; Stepanova, O. V.; Bykova, T. A.; Markin, A. V.; Muzafarov, A. M.; Tatarinova, E. A.; Myakushev, V. D. *Thermochim. Acta* **2006,** 440, 188.
77. Shumilkina, N. A.; Myakushev, V. D.; Tatarinova, E. A.; Gallyamov, M. O.; Khokhlov, A. R.; Buzin, M. I.; Muzafarov, A. M. *Dokl. Chem.* **2005,** 403, 155-159.
78. Karatasos, K.; Adolf, D. B.; Davies, G. R. *J. Chem. Phys.* **2001,** 115, 5310-5318.
79. Moreno, K. X.; Simanek, E. E. *Macromolecules* **2008,** 41, 4108-4114.
80. Sidorenko, A.; Zhai, X. W.; Peleshanko, S.; Greco, A.; Shevchenko, V. V.; Tsukruk, V. V. *Langmuir* **2001,** 17, 5924-5931.

81. Striolo, A.; Prausnitz, J. M. *J. Chem. Phys.* **2001,** 114, 8565-8572.
82. Striolo, A.; Prausnitz, J. M.; Bertucco, A.; Kee, R. A.; Gauthier, M. *Polymer* **2001,** 42, 2579-2584.
83. Zagar, E.; Grdadolnik, J. *J. Mol. Struct.* **2003,** 658, 143-152.
84. Zagar, E.; Huskic, M.; Zigon, M. *Macromol. Chem. Phys.* **2007,** 208, 1379-1387.
85. Baschnagel, J.; Binder, K. *Macromolecules* **1995,** 28, 6808-6818.
86. Gao, Y.; Liu, J.; Zhang, L.; Cao, D. *Macromol. Theor. Simul.* **2013,** 23, 36-48.
87. Eslami, H.; Karimi-Varzaneh, H. A.; Muller-Plathe, F. *Macromolecules* **2011,** 44, 3117-3128.
88. Batistakis, C.; Lyulin, A. V.; Michels, M. A. J. *Macromolecules* **2012,** 45, 7282-7292.
89. Xu, D.-H.; Yuan, J.; Yao, Z.-J.; Zhou, Y.; Gao, J.-H.; Zhang, F.-C. *Phys. Rev. B* **2012,** 86, 201404.
90. Young, R. J.; Kinloch, I. A.; Gong, L.; Novoselov, K. S. *Compos. Sci. Tech.* **2012,** 72, 1459-1476.
91. Aluru, N. R.; Park, J. H. *Surf Sci* **2011,** 605, 1616-1620.
92. Provencher, S., A general-purpose constrained regularization method for inverting photon correlation data. In *Photon Correlation Techniques in Fluid Mechanics*, Schulz-DuBois, E. O., Ed. Springer-Verlag: Berlin, 1983.
93. Provencher, S. *Comp. Phys. Comm.* **1982,** 27, 229.
94. Tanis, I.; Tragoudaras, D.; Karatasos, K.; Anastasiadis, S. H. *J Phys Chem B* **2009,** 113, 5356-5368.
95. Angell, C. A.; Ngai, K. L.; McKenna, G. B.; McMillan, P. F.; Martin, S. W. *J. Appl. Phys.* **2000,** 88, 3113.
96. Ediger, M. D. *Annu. Rev. Phys. Chem.* **2000,** 51, 99–128.
97. Turky, G.; Shaaban, S. S.; Schöenhals, A. *J. Appl. Polymer Sci.* **2009,** 113, 2477-2484.
98. Williams, M. L.; Landel, R. F.; Ferry, J. D. *J. Amer. Chem. Soc.* **1955,** 77, 3701–3707.
99. Rittigstein, P.; Priestley, R. D.; Broadbelt, L. J.; Torkelson, J. M. *Nature Mater.* **2007,** 6, 278-282.
100. Dalakoglou, G. K.; Karatasos, K.; Lyulin, S. V.; Lyulin, A. V. *J. Chem. Phys.* **2007,** 127, Art No 214903.
101. Malmström, E.; Hult, A.; Gedde, U. W.; Liu, F.; Boyd, R. H. *Polymer* **1997,** 38, 4873-4879.
102. Schwartz, G. A.; Bergman R.; J., S. *J. Chem. Phys.* **2004,** 120, 5736-5744.

Table of Contents Graphic

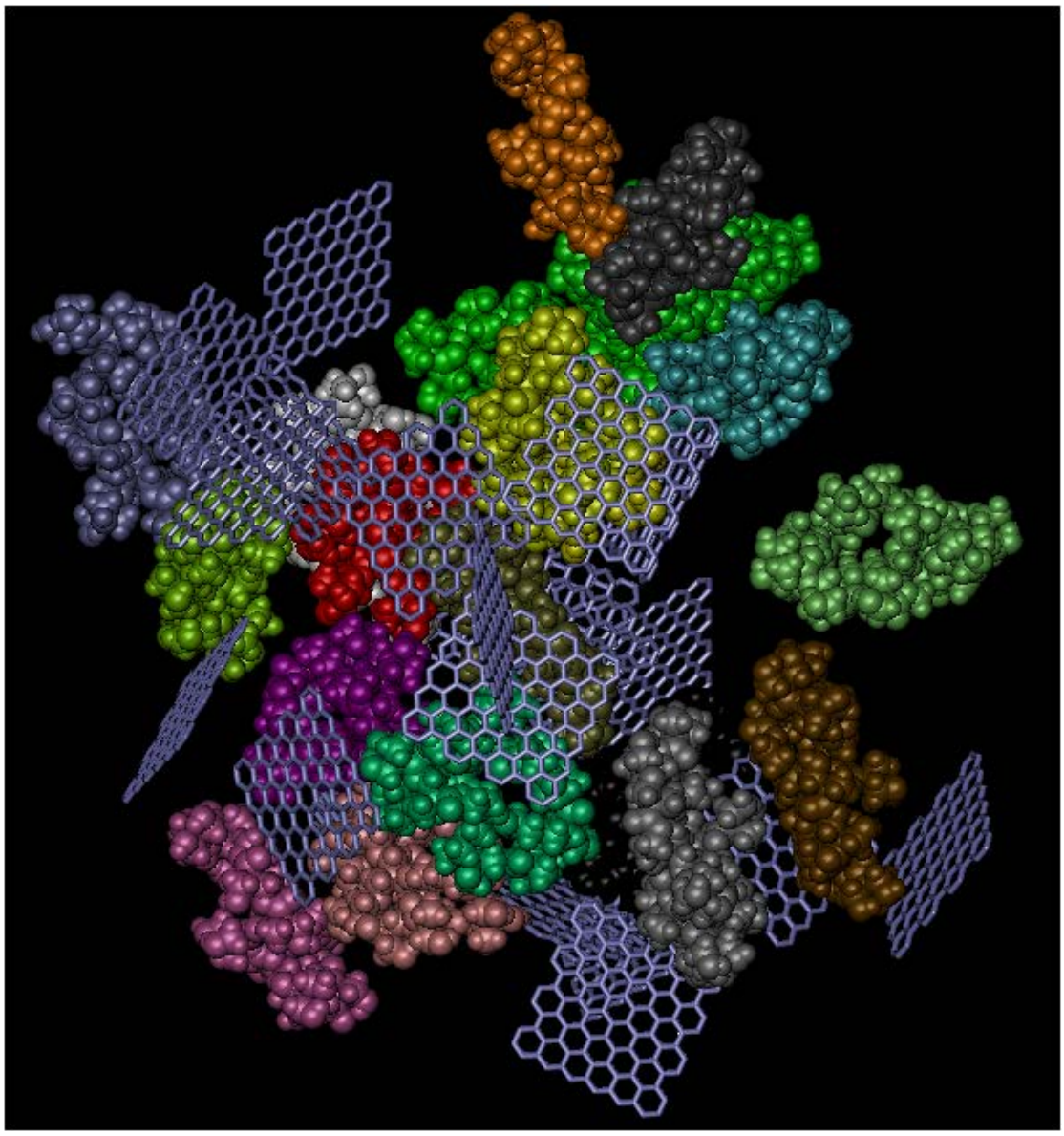

Initial structure of a graphene/hyperebranched polyester nanocomposite. Each polymer molecule appears with a different color for clarity